J|A|C|S
ARTICLES
Published on Web 05/07/2002

Watson−Crick Base-Pairing Properties of Tricyclo-DNA

Dorte Renneberg and Christian J. Leumann*

Contribution from the Department of Chemistry and Biochemistry, University of Bern, Freiestrasse 3, CH-3012 Bern, Switzerland

Received January 11, 2002

Abstract: Tricyclo-DNA belongs to the family of conformationally restricted oligodeoxynucleotide analogues. It differs structurally from DNA by an additional ethylene bridge between the centers C(3′) and C(5′) of the nucleosides, to which a cyclopropane unit is fused for further enhancement of structural rigidity. The synthesis of the hitherto unknown tricyclodeoxynucleosides containing the bases cytosine and guanine and of the corresponding phosphoramidite building blocks is described, as well as a structural description of a representative of an α- and a β-tricyclodeoxynucleoside by X-ray analysis. Tricyclodeoxynucleoside building blocks of all four bases were used for the synthesis of fully modified mixed-base oligonucleotides. Their Watson−Crick pairing properties with complementary DNA, RNA, and with itself were investigated by UV melting curves, CD spectroscopy, and molecular modeling. Tricyclo-DNA was found to be a very stable Watson−Crick base-pairing system. A UV melting curve analysis of the decamers tcd(p**cgtgacagtt**) and tcd(p**aactgtcacg**) showed increased thermal stabilities of up to ΔT_m/mod. = +1.2 °C with complementary DNA and +2.4 °C with complementary RNA. With itself, tricyclo-DNA showed an increase in stability of +3.1 °C/base pair relative to DNA. Investigations into the thermodynamic properties of these decamers revealed an entropic stabilization and an enthalpic destabilization for the tricyclo-DNA/DNA duplexes. CD spectroscopic structural investigations indicated that tricyclo-DNA containing duplexes preferrably exist in an A-conformation, a fact which is in agreement with results from molecular modeling.

Introduction

DNA analogues are of interest in antisense technology to selectively inhibit the gene expression on the level of translation.[1,2] Various mechanisms of inhibition are known, the most important ones being steric blockage or RNase H-induced degradation of the mRNA after duplex formation.[3,4] Several antisense oligonucleotides of the first and second generation are currently being evaluated in clinical trials for the treatment of diseases, for example, various forms of cancer[5] and Crohn's disease.[6] These DNA analogues are typically oligodeoxynucleotide phosphorothioates or 2′-*O*-alkyl-ribooligonucleotides. In 1998, the first antisense drug, the oligodeoxynucleotide phosphorothioate Vitravene (ISIS-2922), became available on the market for use in the treatment of cytomegalovirus (CMV)-induced retinitis. Besides their use in therapy, oligonucleotide analogues also play an increasingly important role in the systematic and high-throughput screening of gene function, and in drug target validation.[7]

In the context of improving the binding properties of antisense oligonucleotides, the concept of conformational restriction of single strands as a means to increase duplex stability has been evaluated within the past decade and has led to DNA analogues with unprecedented thermal duplex stabilities and improved biostability.[8] The locked nucleic acids (LNA)[9−11] and the hexitol nucleic acids (HNA)[12,13] are notable members of this family which show strongly enhanced binding properties to DNA and RNA. The pioneering contribution from our laboratory in this field was the analogue bicyclo-DNA (Figure 1).[14] Homopurine

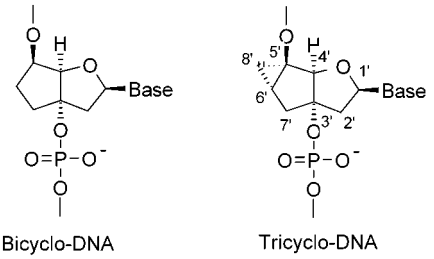

Figure 1. Chemical structures of bicyclo-DNA and tricyclo-DNA.

* To whom correspondence should be addressed. Phone: +41-31-631-4355. Fax: +41-31-631-3422. E-mail: leumann@ioc.unibe.ch.

(1) Myers, K. J.; Dean, N. M. *Trends Pharmacol. Sci.* **2000**, *21*, 19−23.
(2) Uhlmann, E. *Curr. Opin. Drug Discovery Dev.* **2000**, *3*, 203−213.
(3) Baker, B. F.; Monia, B. P. *Biochim. Biophys. Acta* **1999**, *1489*, 3−18.
(4) Crooke, S. T. *Biochim. Biophys. Acta* **1999**, *1489*, 31−44.
(5) Flanagan, W. M. *Cancer Metastatis Rev.* **1998**, *17*, 169−176.
(6) Crooke, S. T. *Antisense Nucleic Acid Drug Dev.* **1998**, *8*, 115−122.
(7) Taylor, M. F.; Wiederholt, K.; Sverdrup, F. *Drug Discovery Today* **1999**, *4*, 562−567.
(8) Leumann, C. J. *Bioorg. Med. Chem.* **2002**, *10*, 841−854.
(9) Koshkin, A. A.; Singh, S. K.; Nielsen, P.; Rajwanshi, V. K.; Kumar, R.; Meldgaard, M.; Olsen, C. E.; Wengel, J. *Tetrahedron* **1998**, *54*, 3607−3630.
(10) Singh, S. K.; Nielsen, P.; Koshkin, A. A.; Wengel, J. *Chem. Commun.* **1998**, 455−456.
(11) Obika, S.; Nanbu, D.; Hari, Y.; Andoh, J.-I.; Morio, K.-I.; Doi, T.; Imanishi, T. *Tetrahedron Lett.* **1998**, *39*, 5401−5404.
(12) Hendrix, C.; Rosemeyer, H.; Verheggen, I.; Seela, F.; Van Aerschot, A.; Herdewijn, P. *Chem.-Eur. J.* **1997**, *3*, 110−120.
(13) Van Aerschot, A.; Verheggen, I.; Hendrix, C.; Herdewijn, P. *Angew. Chem., Int. Ed. Engl.* **1995**, *34*, 1338−1339.
(14) Tarköy, M.; Bolli, M.; Leumann, C. *Helv. Chim. Acta* **1994**, *77*, 716−744.

bicyclo-DNA sequences were shown to form entropically stabilized duplexes with a preference for the Hoogsteen and/or reverse Hoogsteen association mode. This change in association mode relative to DNA was identified to be the consequence of an alteration of the backbone torsion angle γ in the bicyclo-DNA backbone.[15] With mixed-base bicyclo-DNA sequences, Watson−Crick duplex formation with DNA or RNA occurred readily with thermal stabilities near that of DNA duplexes.[16]

Tricyclo-DNA (Figure 1) is a second generation derivative of bicyclo-DNA. The additional cyclopropane ring was designed to confer further conformational stabilization to the nucleoside and eventually a partial correction of the torsion angle γ from the anticlinal range toward the gauche range. Furthermore, the increased hydrophobicity of the tricyclo-DNA backbone is expected to help cellular uptake. We showed previously that homobasic adenine- and thymine-containing tricyclo-DNA oligomers are extraordinarily stable A−T base-pairing systems with a weak preference for the Hoogsteen pairing mode.[17,18] Investigations on the enzymatic stability of tricyclo-DNA proved their resistance against the 3′-exonuclease snake venom phosphodiesterase. Here we report on the synthesis of the hitherto unknown tricyclodeoxycytidine and the tricyclodeoxyguanosine building blocks **5** and **13**, as well as their incorporation into oligodeoxynucleotides. Moreover, X-ray structures of a α- and a β-tricyclodeoxynucleoside, the pairing properties of fully modified tricyclooligonucleotides containing all four bases, a thermodynamic analysis of duplex formation, a CD spectroscopic analysis, and a modeling study of a tricyclo-DNA/DNA duplex are presented.

Results and Discussion

Synthesis of Tricyclodeoxycytidine and Tricyclodeoxyguanosine and Their Phosphoramidite Building Blocks. For nucleoside synthesis the tricyclic sugar derivative **1** (Scheme 1), which had already been prepared in our laboratory, was chosen as starting material.[19] The Me_3SiOTf-induced nucleosidation of **1** with N^4-benzoylcytosine in CH_3CN at 0 °C in the presence of *N*,*O*-bis(trimethylsilyl)acetamide (BSA) afforded **2** in 93% yield as an anomeric mixture of α:β = 1:1. Variation of the reaction temperature did not affect the ratio of anomers. Both anomers could be separated by chromatography after selective removal of the Me_3Si group at C(3′) with TBAF. Unambiguous assignment of the α- and β-configuration in **3** and **4** was possible via ^{1}H NMR difference NOE spectroscopy. In addition, **3** could be crystallized and its structure confirmed by X-ray analysis (vide infra). Treatment of **4** with HF/Et_3N afforded **5** in 90% yield. Selective tritylation of the tertiary OH group at C(5′) was achieved with 4,4′-dimethoxytrityl trifluoromethane sulfonate (DMTOTf)[14] in pyridine in 87% yield. The phosphoramidite building block **7** was obtained by standard reaction of **6** with 2-cyanoethyl *N*,*N*-diisopropyl-chlorophosphoramidite as a 3:2 diastereoisomeric mixture (^{1}H and ^{31}P NMR).

The nucleosidation of the tricyclic sugar **1** with protected guanine was attempted in the same way with Me_3SiOTf as Lewis acid and BSA as the silylating agent. To circumvent the formation of N^7/N^9-mixtures during nucleosidation,[20] we first chose the protected O^6-*p*-nitrophenethyl-N^2-isobutyrylguanine as the base synthon.[21] Unfortunately, in this way only the corresponding α-nucleosides in a N^7/N^9 ratio of 2:1 could be obtained in 65% yield (see Supporting Information).

Scheme 1[a]

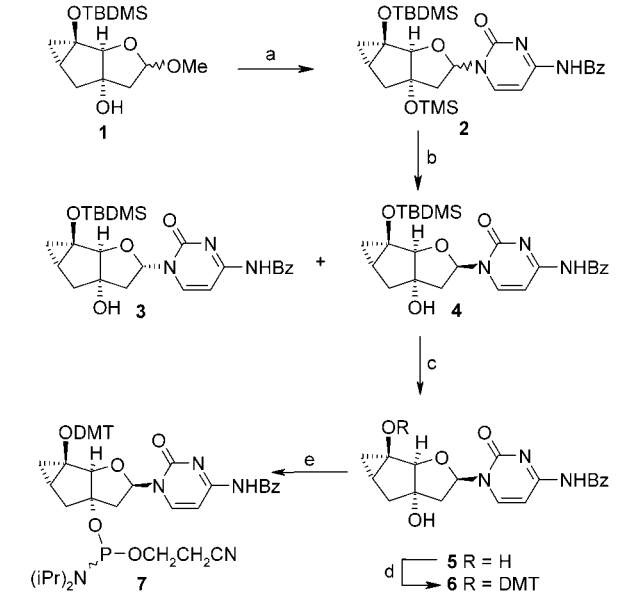

[a] Reagents: (a) N^4-benzoylcytosine, $CF_3SO_3SiMe_3$, BSA, CH_3CN, 0 °C, overnight, 93%; (b) TBAF, THF, 3 min, 84% (both isomers); (c) HF Et_3N, THF, 9 h, 90%; (d) DMTOTf, pyridine, 12 h, 87%; (e) 2-cyanoethyl *N*,*N*-diisopropylchlorophosphoramidite, *N*,*N*-diisopropylethylamine, CH_3CN, 2 h, 91%.

Alternatively, the nucleosidation was realized with O^6-diphenyl-carbamoyl-N^2-isobutyrylguanine as the protected base.[22] Under these conditions, a rewarding N^7/N^9 ratio of 1:9 was obtained from which the two anomers of the N^9-nucleosides, **8** and **9**, were isolated in ca. 24% yield, each (Scheme 2). Elimination of the O^6-diphenyl-carbamoyl protecting group was achieved by heating **9** in a saturated solution of $NaNO_2$ in DMSO to give **11** in 90% yield (Scheme 3).[23] The β-configuration in **11** could be assigned unambiguously by ^{1}H NMR difference NOE spectroscopy, while the N-9 connectivity was warranted by the characteristic chemical shifts of C(4) and C(5) in the ^{13}C NMR spectra.[20] After deprotection of the O(5′)-TBDMS group using HF/Et_3N in THF, the nucleoside analogue **12** became available. The phosphoramidite building block **14** was obtained by selective tritylation of **12** with DMTOTf in pyridine followed by reaction with 2-cyanoethyl *N*,*N*-diisopropylchlorophosphoramidite. ^{1}H and ^{31}P NMR indicated a mixture of two diastereoisomers (at phosphorus) in a ratio of 3:2.

Structure of Tricyclodeoxynucleosides. To investigate constitution and conformation of the tricyclodeoxynucleosides, we subjected crystals of the α-tricyclodeoxycytidine derivative **3** as well as of N^{6Bz}-β-tricyclodeoxyadenosine **15** (obtained as described before[19]) to X-ray structure analysis. In both cases, the expected exo-configuration of the cyclopropane ring and the respective configuration at the anomeric center could be

(15) Bolli, M.; Litten, C.; Schütz, R.; Leumann, C. *Chem. Biol.* **1996**, *3*, 197−206.
(16) Bolli, M.; Trafelet, H. U.; Leumann, C. *Nucleic Acids Res.* **1996**, *24*, 4660−4667.
(17) Steffens, R.; Leumann, C. J. *J. Am. Chem. Soc.* **1999**, *121*, 3249−3255.
(18) Steffens, R.; Leumann, C. J. *J. Am. Chem. Soc.* **1997**, *119*, 11548−11549.
(19) Steffens, R.; Leumann, C. *Helv. Chim. Acta* **1997**, *80*, 2426−2439.
(20) Garner, P. *J. Org. Chem.* **1988**, *53*, 1294−1298.
(21) Jenny, T. *Nucleosides Nucleotides* **1992**, *11*, 1257.
(22) Timar, Z.; Kovács, L.; Kovács, G.; Schmel, Z. *J. Chem. Soc., Perkin Trans. 1* **2000**, 19−26.
(23) Ackermann, D.; Pitsch, S. *Helv. Chim. Acta* **2002**, *85*, in press.

Scheme 2[a]

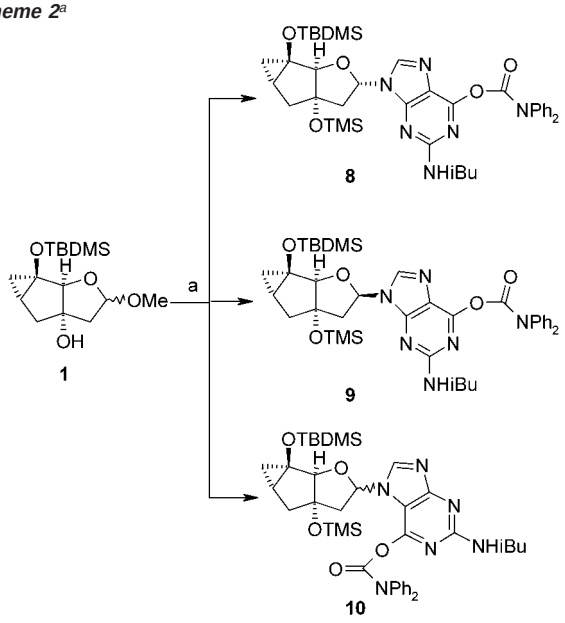

[a] Reagents: (a) O^6-diphenyl-carbamoyl-N^2isobutyrylguanine, CF_3SO_3-$SiMe_3$, BSA, CH_3CN, 50 °C, 3 h, 53%.

Scheme 3[a]

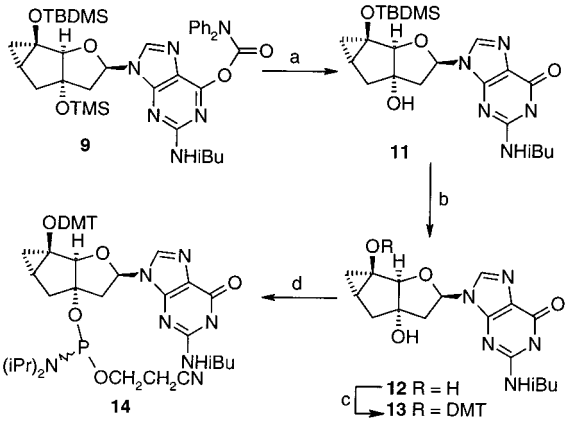

[a] Reagents: (a) sat. $NaNO_2$ in DMSO, 60 °C, 10 h, 90%; (b) HF Et_3N, THF, 8 h, 61%; (c) DMTOTf, pyridine, 10 h, 83%; (d) 2-cyanoethyl *N*,*N*-diisopropylchlorophosphoramidite, *N*,*N*-diisopropylethylamine, CH_3CN, 10 h, 58%.

confirmed (Figure 2). In the α-nucleoside **3**, the furanose ring occurs in a C(3′)-endo conformation (^{3}E, *North*-type). Although there exists a trend for the preference of the C(3′)-exo, the C(4′)-endo, and the C(2′)-exo sugar pucker in α-nucleosides, the C(3′)-endo conformation, as found here, is not unique.[24,25] Values for the backbone relevant torsion angles γ, δ, and χ are summarized in Table 1. Intermolecular contacts in the crystal of **3** arise from H-bonds between N(4)−H···O(3′) and O(3′)−H···N(3).

In the case of the β-nucleoside **15**, the adenine base is syn-oriented ($\chi = 59°$) and kept in this conformation via a intramolecular H-bond between O(5)−H and N(3). This intramolecular H-bond almost certainly influences the conformation of the furanose ring (C(2′)-endo, ^{2}E, *South*-type) and torsion angle γ (Table 1), rendering an extrapolation of the conformation of β-tricyclodeoxynucleoside units within an oligonucleotide chain difficult. It becomes clear, however, that only a marginal

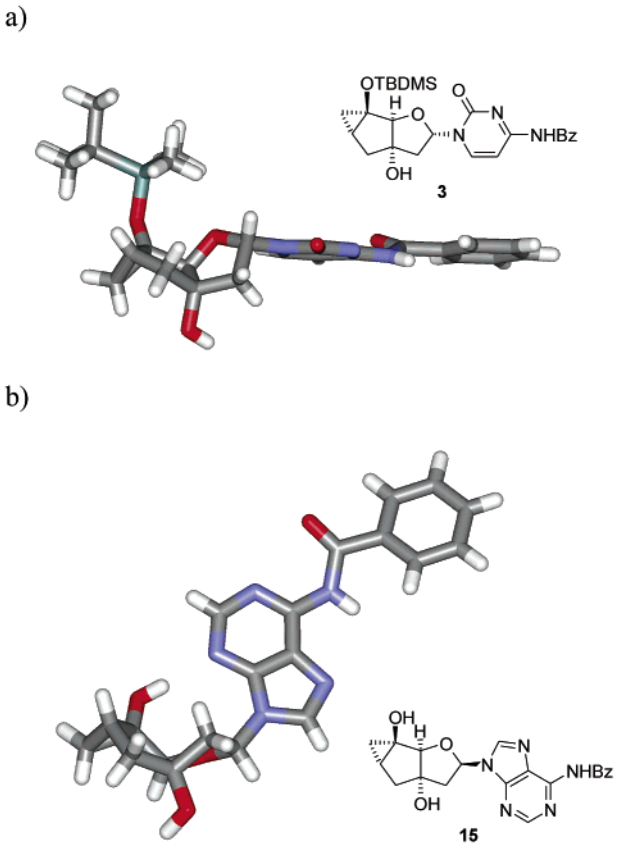

Figure 2. X-ray crystal structures of tricyclodeoxynucleosides: (a) **3** and (b) **15**.

Table 1. Furanose Conformation and Values of Selected Torsion Angles of Tricyclonucleosides **3** and **15**, Bicyclonucleoside β-bcd T,[26] and B-DNA[27]

	3	**15**	β-bcd T	B-DNA
furanose pucker	C(3′)-endo	C(2′)-endo	C(1′)-exo	C(2′)-endo
γ	158°	130°	149°	54°
δ	96°	154°	126°	123°
χ	170°	59°	−113°	−117°

correction of γ, relative to bicyclonucleosides, is achieved by introduction of the cyclopropane ring.

Synthesis of the Oligonucleotides 16−25. Figure 3 gives an overview on the oligonucleotides prepared for the present study. Tricyclodeoxynucleotide phosphoramidites were coupled using standard procedures. The important changes to the typical synthesis protocols were the use of longer coupling times (6−10 min) and the use of 5-(benzylmercapto)-1*H*-tetrazole instead of tetrazole as the activator.

Detritylation was affected as usual (2% trichloroactetic acid, 60 s). Coupling yields were generally >98% according to trityl assay. Oligomers **20** and **21** had to be 5′-phosphorylated, due to the chemical instability of 5′-terminal, unprotected tricyclodeoxynucleoside residues under the conditions of deprotection and cleavage from solid support.[17] For reasons of comparability, the oligomers **16**−**19** and **22**, **23** were also 5′-phosphorylated. Crude oligonucleotides were purified by DEAE ion-exchange HPLC. Their purity was controlled by RP-HPLC before analyzing their structural integrity by ESI-MS spectroscopy (Figure 3).

(24) Sundaralingam, M. *J. Am. Chem. Soc.* **1971**, *93*, 6644−6647.
(25) Swarna, L. Y.; Yathindra, N. *Biopolymers* **1992**, *32*, 249−266.

Table 2. T_m and ΔT_m Values (°C) from UV Melting Curves (260 nm)[a]

	DNA complement				RNA complement			
	(150 mM NaCl)		(1 M NaCl)		(150 mM NaCl)		(1 M NaCl)	
	T_m	ΔT_m[b]	T_m	ΔT_m[b]	T_m	ΔT_m[c]	T_m	ΔT_m[c]
23: d(pAACTGTCACG)	44.4		49.4		42.5		47.8	
16: d(pAACTGT **c** ACG)	46.8	+2.4	52.5	+3.1	45.7	+3.2	49.8	+2.0
17: d(pAACTG **t** CACG)	45.3	+0.9	51.4	+2.0	43.0	+0.5	48.2	+0.4
18: d(pAACTGTC **a** CG)	43.4	−1.0	49.1	−0.3	42.1	−0.4	47.0	−0.8
19: d(pAACT **g** TCACG)	44.7	+0.3	50.4	+1.0	43.5	+1.0	47.7	−0.1

[a] 10 mM NaH_2PO_4, pH 7.0, $c = 2$ μM. [b] Values relative to DNA/DNA duplex. [c] Values relative to DNA/RNA duplex.

Table 3. T_m and ΔT_m Values (°C) from UV Melting Curves (260 nm) in a 150 mM NaCl (1 M NaCl in parentheses)[a]

	22: d(pCGTGACAGTT)		**20**: tcd(**pcgtgacagtt**)		**24**: r (CGUGACAGUU)	
	T_m	ΔT_m/mod.	T_m	ΔT_m/mod.	T_m	ΔT_m/mod.
23: d(pAACTGTCACG)	44.4 (49.4)		57.2 (62.8)	+1.2 (+1.3)	42.5 (47.8)	
21: tcd(p**aactgtcacg**)	55.2 (62.7)	+1.1 (+1.3)	75.2 (∼80)	+3.1 (+3)	61.6 (67.6)	+1.9 (+2.0)
25: r(AACUGUCACG)	40.1 (46.0)		64.8 (69.5)	+2.4 (+2.4)	52.2 (57.5)	

[a] 10 mM NaH_2PO_4, pH 7, $c = 2$ μM.

		[M-H]$^-$ calc.	[M-H]$^-$ found
16	d (pAACTGT **c** ACG)	3129.9	3129.3
17	d (pAACTG **t** CACG)	3129.9	3128.7
18	d (pAACTGTC **a** CG)	3129.9	3128.7
19	d (pAACT **g** TCACG)	3129.9	3128.7
20	tcd (p **c g t g a c a g t t**)	3503.2	3503.1
21	tcd (p **a a c t g t c a c g**)	3472.1	3472.2
22	d (pCGTGACAGTT)	3121.5	3121.5
23	d (pAACTGTCACG)	3090.5	3090.3
24	r (CGUGACAGUU)	3160.8	3160.6
25	r (AACUGUCACG)	3143.8	3143.5

Figure 3. Sequences of tricyclodeoxynucleoside containing oligonucleotides and their corresponding mass-spectrometric data (**a** = tricyclodeoxyadenosine; **c** = tricyclodeoxycytosine; **g** = tricyclodeoxyguanosine; **t** = tricyclothymidine).

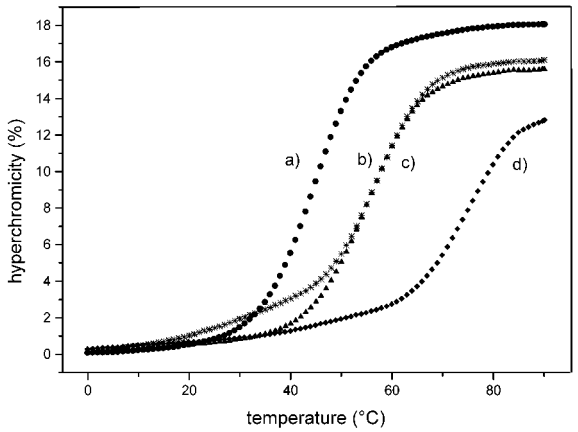

Figure 4. UV melting curves (260 nm) of DNA/DNA, DNA/tricyclo-DNA, and tricyclo-DNA/tricyclo-DNA duplexes: (a) **22/23**, (b) **20/23**, (c) **21/22**, (d) **20/21** in 10 mM NaH_2PO_4, pH 7, 150 mM NaCl, $c = 2$ μM.

Duplex Formation of Oligonucleotides Containing Single Tricyclodeoxynucleotide Units with DNA and RNA. Complementary pairing experiments of the sequences **16**−**19** were carried out with DNA as well as RNA. The duplex formation was monitored by UV melting curve analysis (260 nm). The melting temperatures (T_m) are summarized in Table 2.

From these data, it appears that single substitutions of the four different tricyclodeoxynucleotide units within the oligomer showed subtle but distinct differences in T_m relative to the natural oligodeoxynucleotide. The oligonucleotide **16**, containing a tricyclodeoxycytidine unit, shows the highest increase in T_m. At 150 mM NaCl, a ΔT_m of +2.4 °C with DNA and of +3.2 °C with RNA as the complement was measured. Duplexes containing a tricyclodeoxythymine or tricyclodeoxyguanosine unit still showed increased T_m (+0.3 to +1.0 °C), while incorporation of a tricyclodeoxyadenosine unit leads to a duplex with slightly decreased stability (−0.4 to −1.0 °C) relative to the unmodified duplex. The observed differences in stability might be either due to differential structural effects intrinsic to the tricyclo-modification or due to differential nearest neighbor effects in the sequence. As a general picture, it emerges that tricyclopyrimidine nucleotides stabilize duplex formation with complementary DNA and RNA more than tricyclopurine nucleosides. A possible rationalization of this observation invokes the intrinsically weaker intrastrand stacking of pyrimidine bases that is compensated more efficiently by the rigid backbone in tricyclo-DNA, relative to DNA.

Duplex Formation of Fully Modified Oligotricyclodeoxynucleotides with DNA and RNA. To determine the ability of tricyclo-DNA to form stable Watson−Crick duplexes, fully modified tricyclo-DNA oligonucleotides containing all four bases in a random distribution were examined. Complementary pairing experiments of tricyclo-DNA oligonucleotides **20**, **21** were carried out in their own series and with natural DNA and RNA at low (150 mM) and high (1 M) NaCl concentration. To exclude self-pairing of **20** or **21**, a UV melting experiment of oligonucleotide **20** without complement was performed. As expected, no cooperative melting transition at the temperature interval of 0−90 °C could be observed, indicating the absence of self-association.

The melting temperatures and the corresponding melting curves for duplexes with complementary DNA are depicted in Table 3 and Figure 4. Both duplexes containing one tricyclo-DNA strand, **20/23** and **21/22**, show increased melting temperatures with a ΔT_m of +11−12 °C as compared to the natural systems. Thus, the stabilization per modification (ΔT_m/mod.) amounts to +1.2 °C. In its own series, tricyclo-DNA constitutes

Table 4. T_m and ΔT_m Values of Mismatched versus Matched Duplexes within the Backbone Series Tricyclo-DNA, DNA, and RNA, against RNA as a Target (10 mM NaH_2PO_4, 150 mM NaCl, pH 7.0, $c = 2$ μM)

	r(UUGACX**G**UGC)						
	X = A	X = U		X = G		X = C	
	T_m	T_m	ΔT_m	T_m	ΔT_m	T_m	ΔT_m
24 (RNA)	52.2 °C	39.5 °C	−12.7 °C	50.6 °C	−1.6 °C	39.2 °C	−13.0 °C
22 (DNA)	42.5 °C	27.5 °C	−15.0 °C	40.4 °C	−2.1 °C	28.0 °C	−14.5 °C
20 (tc-DNA)	61.6 °C	44.1 °C	−17.5 °C	59.0 °C	−2.6 °C	46.0 °C	−15.6 °C

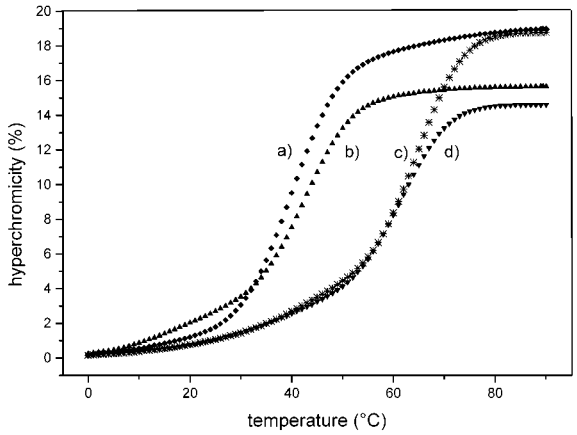

Figure 5. UV melting profiles (260 nm) of DNA/RNA and tricyclo-DNA/RNA duplexes: (a) **22/25**, (b) **23/24**, (c), **20/25**, (d) **21/24** in 10 mM NaH_2PO_4, pH 7, 150 mM NaCl, $c = 2$ μM single strand concentration.

the most stable pairing systems with a T_m of 75 °C for the decamer duplex **20/21** (ΔT_m of +31 °C). As expected, higher salt concentration leads to higher melting temperatures for all duplexes. No differential effects between DNA and the tricyclo-DNA were observed, indicating a similar dependence of T_m on electrolyte concentration.

With complementary RNA, duplex stabilization was even more pronounced. As extracted from Table 3 and Figure 5, both tricyclo-DNA/RNA heteroduplexes show a considerably higher T_m as compared to the natural hybrid. For the duplex **20/25**, an increase in stability of more than 24 °C was observed which results in a ΔT_m/mod. = +2.4 °C. Remarkably, the heteroduplexes formed between tricyclo-DNA and RNA are more stable than the corresponding natural RNA duplex by ca. 10−12 °C.

Mismatch Discrimination in Tricyclo-DNA/DNA and Tricyclo-DNA/RNA Duplexes. To analyze the base selectivity in RNA recognition by tricyclo-DNA, we investigated the duplexes between complementary RNA, containing one mismatched base in the center of the sequence, with **20** (tricyclo-DNA) and compared it to those with **22** (DNA) and **24** (RNA). As can be seen from the ΔT_m values in Table 4, any mismatched base arrangement in the tricyclo-DNA/RNA hybrid duplexes is associated with a dramatic decrease in T_m giving rise to ΔT_m values of −17.5 °C for the T−U and −15.6 °C for the T−C arrangement relative to the standard T−A base pair. As expected, the T−G wobble base pair is only slightly less stable than the matched T−A base pair in all cases investigated. Considering the various backbones involved, relative mismatch discrimination is largest in the tricyclo-DNA/RNA hybrids intermediate in the DNA/RNA hybrids and lowest in the RNA duplexes. From these experiments, it appears that tricyclo-DNA does not only recognize complementary RNA with increased thermal stability, but also with increased selectivity.

Analysis of the Helix Conformation of Tricyclooligonucleotide Duplexes. A CD spectroscopic analysis of tricyclodeoxyoligonucleotide-containing duplexes was performed to investigate the structural preferences. CD spectra above and below the melting temperature were recorded for the pure tricyclo-DNA duplex **20/21**, the tricyclo-DNA/DNA hybrid duplexes **21/22** and **20/23**, the tricyclo-DNA/RNA hybrid **21/24**, as well as for the control DNA duplex **22/23**, and the DNA/RNA duplex **23/24** (Figure 6).

In the nondenatured state, the CD spectra of the pure tricyclo-DNA or the DNA/tricyclo-DNA duplexes (B, C, D) show hypsochromic shifts of the ellipticity maximum by about 9−17 nm, relative to the DNA duplex (A). In all these cases, only a minor change in intensity of the negative minimum ellipticity at ca. 240 nm is observed upon denaturation, which is in contrast to the spectra of the pure DNA duplex. The proportion of the intensity of the positive over the negative maximum is in the range from 2:1 to 4:1 in the tricyclo-DNA-containing duplexes, while it is slightly less than 1:1 for the DNA duplex. The CD spectra of the pure tricyclo-DNA duplex (B) and the tricyclo-DNA hybrid duplexes (C, D) are thus reminiscent of a helix of the A-conformation, while that of the DNA duplex (A) showed, as expected, all of the characteristics of a B-helix. The CD spectra of the corresponding RNA/tricyclo-DNA duplex (F) are very similar to that of the RNA/DNA reference spectra, indicating again A-conformation of the helices. The structural preference of tricyclo-DNA for A-type double helices is in line with the enhanced stability of tricyclo-DNA/RNA duplexes relative to tricyclo-DNA/DNA duplexes.

Molecular Dynamics Simulation. The preference of tricyclo-DNA/DNA duplexes for the A-conformation, as determined by CD spectroscopy, prompted us to perform a molecular dynamics simulation of the duplex **21/22** to get independent support and to determine the backbone parameters. The simulation started from a duplex in B-DNA geometry and resulted after a 200 ps trajectory in a double helical structure which strongly resembles that of an A-form helix. An average structure of the last 50 ps of the internal six base pairs of the decamer is depicted in Figure 7. For comparison, the corresponding bicyclo-DNA/DNA duplex of the same sequence was analyzed in analogy. The structural evaluation of the two systems shows an interesting picture concerning the six torsion angles describing the repeating unit of the phosphodiester backbone (Table 5) and highlights the structural effect of the cyclopropane ring on the bicyclic core system.

The phosphodiester bonds in the tricyclo-DNA strand (torsion angle α and ζ) are in a trans/gauche arrangement and thus differ from those of the other duplexes. A remarkable change was found for the torsion angle β which shows values of 87° in tricyclo-DNA. This is in contrast to the ca. 180° typically observed in A- or B-DNA. The furanose ring prefers a O(4′)-

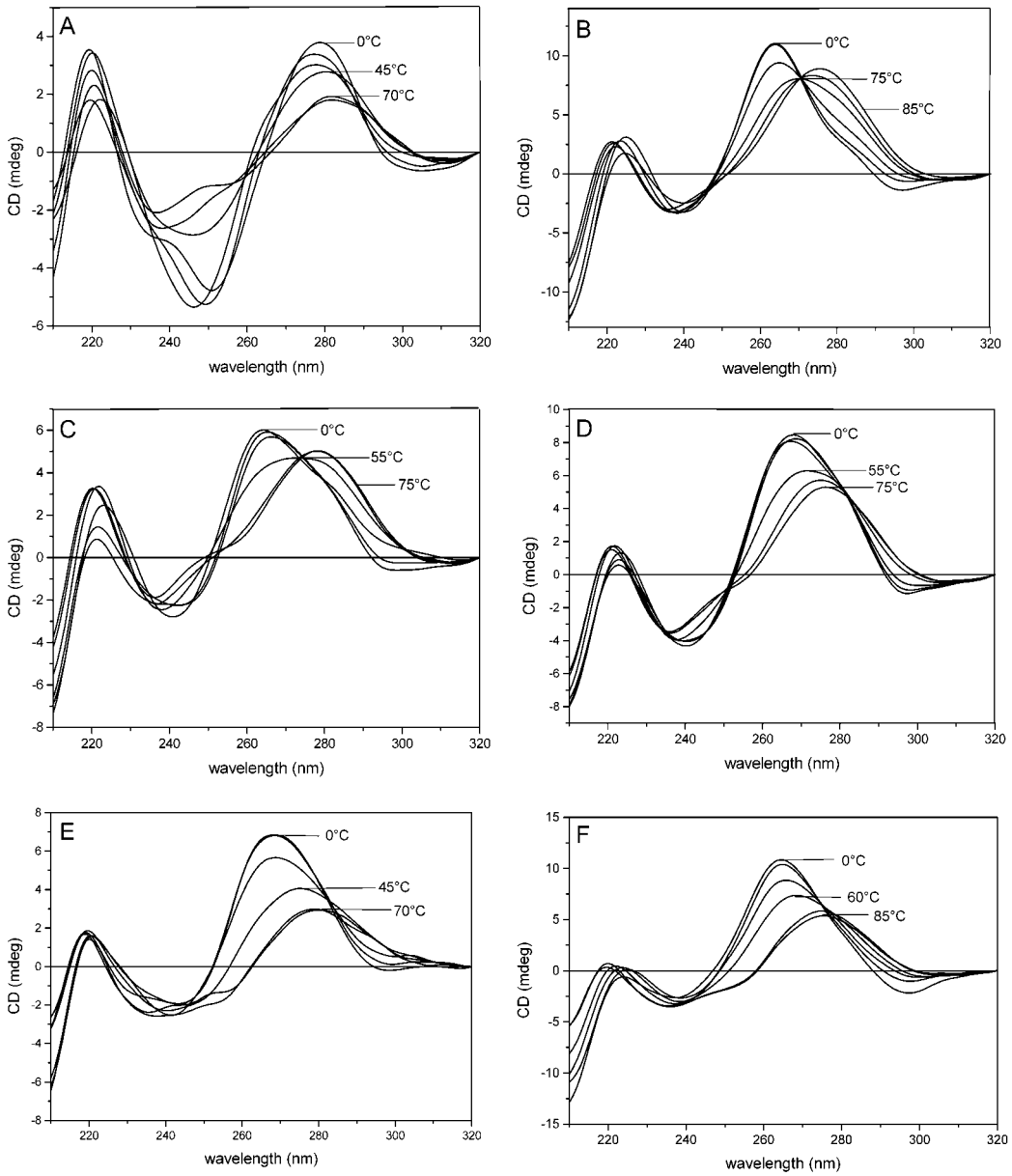

Figure 6. CD traces of duplexes containing DNA and tricyclo-DNA strands at different temperatures: (A) **22/23**; (B) **20/21**; (C) **20/23**; (D) **21/22**; (E) **23/24**; (F) **21/24** in 10 mM NaH_2PO_4, 150 mM NaCl, pH 7, $c = 2$ μM.

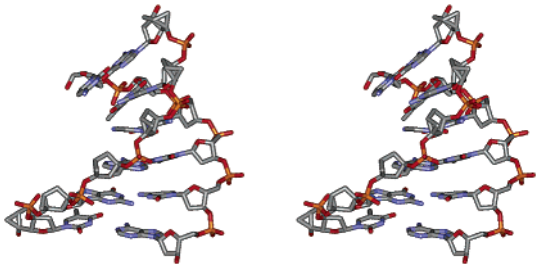

Figure 7. Stereoscopic view of the averaged structure of the last 50 ps of the 200 ps molecular dynamics simulation (Insight II/Discover) of the six central base pairs of the duplex **21/24**.

Table 5. Backbone Torsion Angles $\alpha-\zeta$ for A- and B-DNA as well as for Bicyclo-DNA and Tricyclo-DNA in Complex with Natural DNA, Determined by Molecular Modeling

torsion angles	A-DNA[a]	B-DNA[a]	bicyclo-DNA	tricyclo-DNA
α	$-75° \pm 36$	$-63° \pm 8$	$-166° \pm 2$	$-156° \pm 10$
β	$-175° \pm 13$	$171° \pm 14$	$178° \pm 2$	$87° \pm 6$
γ	$56° \pm 22$	$54° \pm 8$	$143° \pm 4$	$149° \pm 10$
δ	$91° \pm 18$	$123° \pm 21$	$122° \pm 3$	$92° \pm 7$
ϵ	$-166° \pm 19$	$-169° \pm 25$	$177° \pm 3$	$173° \pm 8$
ζ	$-75° \pm 19$	$-108° \pm 34$	$-86° \pm 4$	$23° \pm 6$

[a] Data taken from ref 27.

endo conformation. The torsion angle $\gamma = 149°$ is in the anti orientation, while $\delta = 92°$ is in a gauche arrangement, as observed for A-DNA. The structural differences of the modeled tricyclo-DNA units in the furanose pucker and torsion angles γ and δ with those discernible from the X-ray crystal structure of the tricyclodeoxynucleoside **15** are best explained by the structural bias originating from the syn orientation of the adenine base enforced via intramolecular H-bonding (vide supra) in the crystal of **15**.

From comparison of the data of bicyclo- and tricyclo-DNA, it appears that the cyclopropane ring has an astonishingly minor effect on torsion angle γ. However, it drives the furanose ring of the bicyclic core system preferentially into a C(3′)-endo-

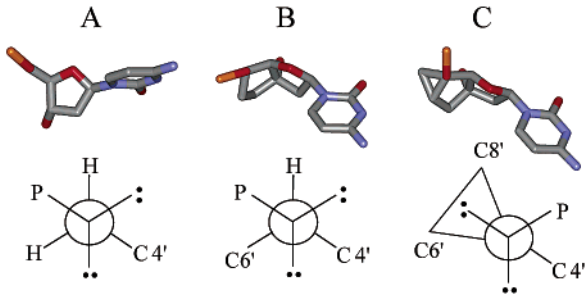

Figure 8. Nucleoside units and idealized Newman projections along the O(5′)−C(5′) bond (torsion angle β) of the averaged structures as obtained from molecular modeling: (A) B-DNA; (B) bicyclo-DNA; (C) tricyclo-DNA.

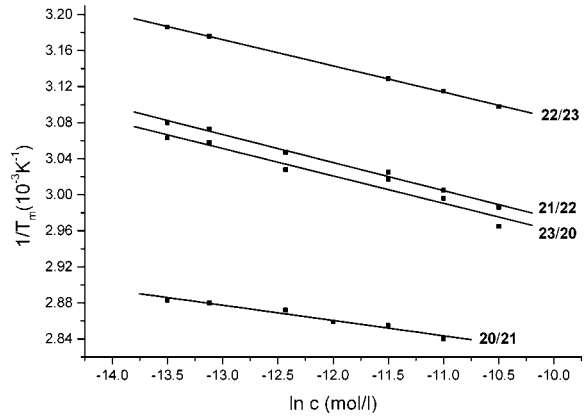

Figure 9. $1/T_m$ vs ln(c) plots of the four duplex systems (10 mM NaH_2PO_4, 150 mM NaCl, pH 7.0).

like conformation and is responsible for the observed change in torsion angle β. A conformational analysis around the O(5′)−C(5′) bond illustrates that in tricyclo-DNA the gauche arrangement of β is preferred over the typical trans arrangement, due to the steric constraints imposed by the cyclopropane ring (Figure 8). We assume that the preferential change of β from trans to gauche going from bicyclo- to tricyclo-DNA is responsible for the improved Watson−Crick base-pairing properties of the latter system. Although four out of six backbone torsion angles differ appreciably from that of A-DNA (or RNA), the overall shape of the double helix still preserves an A-like character, a fact that is fully supported by the CD spectroscopic investigations. Thus, tricyclo-DNA, in contrast to bicyclo-DNA, is a structural mimic of RNA and not of DNA.

Thermodynamic Data of Duplex Formation. Thermodynamic data of duplex formation were obtained from DNA melting curves by the concentration variation method.[28] The data obtained from the $1/T_m$ versus ln(c) plots of the four duplex systems (Figure 9) are summarized in Table 6. The calculated standard enthalpies of duplex formation $\Delta G^{25\,°C}$ are in complete agreement with the observed thermal stabilities of the four systems. The two tricyclo-DNA/DNA duplexes show an entropic stabilization along with an enthalpic destabilization, relative to the natural system. However, the pure tricyclic duplex behaves differently. Here the stability appears to be largely enthalpy driven. Although it is tempting to interpret the data in terms of less strain in the duplex with the homostructural tricyclo-backbone, one cannot exclude at this point whether the data are biased by non-two-state model behavior of tricyclo-DNA duplex melting. For clarification, model independent thermodynamic data, as, for example, from calorimetric experiments, are necessary.

Table 6. Thermodynamic Data of Duplex Formation Determined from the $1/T_m$ versus ln(c) Plots in a 10 mM NaH_2PO_4, 150 mM NaCl, pH 7 Buffer

	ΔH (kcal/mol)	ΔS (cal/mol K)	$\Delta G^{25\,°C}$ (kcal/mol)
DNA **22**/DNA **23**	−68.2	−187.8	−12.2
DNA **23**/tc-DNA **20**	−63.8	−167.2	−14.0
tc-DNA **21**/DNA **22**	−65.4	−170.8	−14.5
tc-DNA **20**/tc-DNA **21**	−117.0	−308.1	−25.2

Conclusions

Fully modified tricyclo-DNA sequences form remarkably stable duplexes with DNA as well as with RNA. The average increase in melting temperature was determined to be +1.2 °C/mod. with complementary DNA and +2.4 °C/mod. with complementary RNA. The most stable duplexes, however, are formed in the pure tricyclo-DNA series with ΔT_m values of +3.1 °C/base pair relative to DNA. Base−base recognition is highly selective in tricyclo-DNA/RNA duplexes and is superior to that of pure RNA and DNA/RNA duplexes. In the homoadenine−homothymine sequence context, tricyclo-DNA can show increases in T_m of up to +4 °C/mod. In the latter cases, however, the Hoogsteen pairing modus is preferred over the Watson−Crick base-pairing modus. In comparison to other conformationally restriced oligonucleotide analogues, tricyclo-DNA shows higher RNA affinity as the recently introduced CeNA[29] and is only slightly superseded by the analogue HNA,[12,13] which displays increases in T_m of +1.3 °C/mod. with complementary DNA and +3 °C/mod. with RNA. With respect to LNA,[9,11] about one-half of the increase in thermal stability (ΔT_m/mod. = 4−8 °C against RNA) can be gained. Tricyclo-DNA also shows enhanced binding efficiency relative to DNA analogues with charge neutral backbones, as PNA[30] or the morpholino-DNA.[31]

In comparison to bicyclo-DNA, a remarkably higher propensity for Watson−Crick duplex formation is found for tricyclo-DNA. A molecular modeling study and CD spectroscopic analysis of a tricyclo-DNA/DNA duplex revealed a strong preference for an A-type helix, assigning tricyclo-DNA, in contrast to bicyclo-DNA, the character of an RNA mimic. In the absence of high-resolution structural data, it appears from molecular modeling and CD spectroscopy that the cyclopropane ring drives the furanose unit into a N-type conformation and torsion angle β into a gauche instead of trans arrangement. These changes seem to be primarily responsible for the overall A-helix shape of duplexes and for the enhanced stability of Watson−Crick duplexes relative to bicyclo-DNA. Alternatively, the higher hydrophobicity of the tricyclo-DNA system along with

(26) Tarköy, M.; Bolli, M.; Schweizer, B.; Leumann, C. *Helv. Chim. Acta* **1993**, *76*, 481−510.
(27) Saenger, W. *Principles of Nucleic Acid Structure*; Springer-Verlag: New York, 1984.
(28) Marky, L. A.; Breslauer, K. J. *Biopolymers* **1987**, *26*, 1601−1620.
(29) (a) Wang, J.; Verbeure, B.; Luyten, I.; Lescrinier, E.; Froeyen, M.; Hendrix, C.; Rosemeyer, H.; Seela, F.; Van Aerschot, A.; Herdewijn, P. *J. Am. Chem. Soc.* **2000**, *122*, 8595−8602. (b) Verbeure, B.; Lescrinier, E.; Wang, J.; Herdewijn, P. *Nucleic Acids Res.* **2001**, *29*, 4941−4947.
(30) Uhlmann, E.; Peyman, A.; Breipohl, G.; Will, D. W. *Angew. Chem., Int. Ed.* **1998**, *37*, 2796−2823.
(31) Summerton, J. E. *Biochim. Biophys. Acta* **1999**, *1489*, 141−158.

a differential hydration behavior of the helix, relative to bicyclo-DNA, could also be in part responsible for the observed differences in the hybridization properties.

In conclusion, with its favorable DNA and RNA binding properties, tricyclo-DNA definitely represents an interesting candidate worthy of further exploration. The investigation of its antisense properties in vitro and in vivo will be the subject of a following communication.

Experimental Section

General. ^{1}H NMR (300, 400, or 500 MHz) and ^{13}C NMR (75, 100, or 125 MHz) spectra were recorded on a Bruker AC-300, AMX-400, or DRX500 spectrometer. ^{31}P NMR spectra were measured on Bruker DRX500 using 85% H_3PO_4 (=0 ppm) as external standard. Infrared (IR) spectra were obtained using a Perkin-Elmer FTIR 1600 spectrometer. Electron ionization (EI) mass spectral analyses were recorded on a Varian MAT CH-7A; LSIMS on Micromass Autospec Q, matrix: 3-nitrobenzyl alcohol; ESI-MS on VG platform Fisons Instruments, Single Stage Quadrupole ES-MS; and ESI-TOF-MS on Applied Biosystems/Sciex QSTAR Pulsar (QqTOF) mass spectrometer. Flash chromatography was performed using silica gel with an average particle size of 40 μm. Chemicals, solvents, and reagents for reactions were generally obtained from Fluka AG (Buchs, Switzerland), and were of the highest quality available. All reactions were carried out under Ar.

(5′*R*)-(*N*^{4}-Benzoyl-1-[3′-*O*-trimethylsilyl-5′-*O*-(*tert*-butyldimethylsilyl)-2′-deoxy-3′-*C*, 5′-*C*-[(5′-*C*, 6′-*C*-methano)ethano]-D-ribofuranosyl]cytosine (2). To a suspension of *N*^{4}-benzoylcytosine (418 mg, 1.94 mmol) in CH_3CN (9 mL) was added BSA (*N*,*O*-bis(trimethylsilyl)-acetamide; 0.79 mL, 3.22 mmol). After stirring for 1 h at room temperature, a solution of **1** (194 mg, 0.64 mmol) in CH_3CN (5 mL) at 0 °C was added followed by $CF_3SO_3SiMe_3$ (0.35 mL, 1.94 mmol). After stirring for 4 h at 0 °C, another portion of $CF_3SO_3SiMe_3$ (0.05 mL, 0.32 mmol) was added, and the reaction mixture was left overnight at 4 °C. The solution was diluted with EtOAc and extracted with saturated $NaHCO_3$. The organic layer was dried over $MgSO_4$ and concentrated. Flash chromatography (hexane/EtOAc 1:4) of the residue afforded 313 mg (87%) of **2** as a white foam in an anomeric mixture α:β 1:1, besides 12 mg (4%) of **3** and 5 mg (2%) of **4** as colorless oils. Data of **2**: R_f 0.44 (hexane/EtOAc 1:4). ^{1}H NMR (300 MHz, $CDCl_3$): δ 0.04 (s, 6H), 0.06 (s, 6H), 0.12 (s, 9H), 0.14 (s, 9H), 0.80 (m, 1H), 0.86 (s, 9H), 0.90 (s, 9H), 1.00 (m, 3H), 1.36, 1.54 (2m, 2H), 1.70 (m, 3H), 2.07 (dd, 1H, J_1 = 6.0, J_2 = 13.6 Hz), 2.28 (dd, 1H, J_1 = 5.2, J_2 = 13.9 Hz), 2.70 (m, 2H), 2.95 (dd, 1H), 4.28 (s, 1H), 4.32 (s, 1H), 6.09 (m, 2H), 7.50 (m, 8H), 7.89 (d, 4H, J = 7.0 Hz), 8.07 (d, 1H, J = 7.4 Hz), 8.70 (d, 1H), 8.87 (br, 2H). ^{13}C NMR (75 MHz, $CDCl_3$): δ −3.80, −3.77, −3.71, 1.81, 1.85, 16.75, 18.69, 17.80, 23.91, 24.43, 25.65, 39.49, 42.09, 47.23, 47.41, 64.75, 65.15, 87.77, 87.88, 88.23, 90.63, 91.66, 93.94, 95.41, 96.21, 127.45, 127.50, 128.94, 128.95, 133.04, 143.64, 145.34, 162.20, 162.38. IR (film): 3007, 1652, 1478 cm^{-1}. MS (EI): *m*/*z* (rel intensity) 556 (15), 341 (30), 297 (30), 216 (100).

(5′*R*)-(*N*^{4}-Benzoyl-1-[5′-*O*-(*tert*-butyldimethylsilyl)-2′-deoxy-3′-*C*, 5′-*C*-[(5′-*C*, 6′-*C*-methano)ethano]-D-ribofuranosyl]cytosine (3 and 4). A solution of **2** (360 mg, 0.64 mmol) in THF (6 mL) and Bu_4NF (0.68 mL, 0.68 mmol, 1 M in THF) was stirred for 3 min. The reaction was stopped by the addition of H_2O, and the aqueous phase was extracted with EtOAc. The combined organic phases were dried over $MgSO_4$ and concentrated. Flash chromatography (EtOAc) afforded 133 mg (43%) of **3** as a white solid and 128 mg (41%) of **4** as a white foam. Crystals of **3** suitable for X-ray structure determination were obtained from EtOAc. Data of **3**: R_f 0.27 (EtOAc). ^{1}H NMR (300 MHz, CD_3OD): δ 0.17, 0.21 (2s, 6H), 0.91 (s, 9H), 0.97 (m, 1H), 1.05 (m, 1H), 1.62 (m, 1H), 1.70 (d, 1H, J = 13.6 Hz), 2.27 (dd, 1H, J_1 = 6.3, J_2 = 13.6 Hz), 2.35 (dd, J_1 = 4.8, J_2 = 13.6 Hz), 2.84 (dd, 1H, J_1 = 6.3, J_2 = 13.6 Hz), 4.45 (s, 1H), 6.22 (t, 1H, J = 6.3 Hz), 7.27 (d, 1H, J = 7.7 Hz), 7.61, 7.72 (2m, 3H), 8.06 (d, 2H, J = 7.0 Hz), 8.43 (d, 1H, J = 7.7 Hz). ^{1}H NMR-difference-NOE: 4.45 (s, 1H) → 8.43 (d, 1H, J = 7.7 Hz); 6.22 (t, 1H, J = 6.3 Hz) → 2.27 (dd, 1H, J_1 = 6.3, J_2 = 13.6 Hz), 2.84 (dd, 1H, J_1 = 6.3, J_2 = 13.6 Hz); 8.43 (d, 1H, J = 7.7 Hz) → 4.45 (s, 1H), 6.22 (t, 1H, J = 6.3 Hz), 7.27 (d, 1H, J = 7.7 Hz). ^{13}C NMR (75 MHz, CD_3OD): δ −3.22, −3.07, 19.08, 19.33, 25.85, 26.56, 41.20, 48.65, 66.95, 87.28, 89.72, 91.93, 99.04, 129.62, 130.24, 134.69, 134.83, 146.44, 158.21, 164.68, 169.64. MS (ESI-TOF): *m*/*z* (rel intensity) 482.20, 148.95. Data of **4**: R_f 0.15 (EtOAc). ^{1}H NMR (300 MHz, CD_3OD): δ 0.22, 0.30 (2s, 6H), 0.92 (m, 1H), 0.99 (s, 9H), 1.15 (m, 1H), 1.46 (m, 1H), 1.72 (d, 1H, J = 14.3 Hz), 1.84 (dd, 1H, J_1 = 4.4, J_2 = 14.3 Hz), 2.69 (m, 2H), 4.38 (s, 1H), 6.13 (d, 1H, J = 6.3 Hz), 7.57 (m, 3H), 7.60 (m, 1H), 8.04 (d, 2H, J = 7.0 Hz), 8.87 (d, 1H, J = 7.4 Hz). ^{1}H NMR-difference-NOE: 8.87 (d, 1H, J = 7.4 Hz) → 1.46 (m, 1H), 6.13 (d, 1H, J = 6.3 Hz), 7.57 (m, 3H). ^{13}C NMR (300 MHz, CD_3OD): δ −3.21, −3.15, 18.11, 18.99, 26.01, 26.49, 42.91, 49.12, 67.12, 87.10, 92.11, 94.14, 97.73, 129.46, 130.11, 134.38, 134.98, 146.51, 157.93, 165.25, 169.43. IR (film): 3397, 1652, 1482, 1304 cm^{-1}. MS (LSIMS): *m*/*z* (rel intensity) 484 (17), 330 (20), 225 (29), 216 (100). HRMS (LSIMS): *m*/*z* calcd for $C_{25}H_{34}N_3O_5Si$, 484.2267; found, 484.2266.

(5′*R*)-(*N*^{4}-Benzoyl-1-[2′-deoxy-3′-*C*, 5′-*C*-[(5′-*C*, 6′-*C*-methano)-ethano]-β-D-ribo-furanosyl]cytosine (5). To a solution of **4** (115 mg, 0.24 mmol) in THF (3 mL) was added HF Et_3N (0.16 mL, 0.36 mmol). After 6 h and 7 h, further portions of 0.5 equiv of HF Et_3N were added. After 9 h, the reaction mixture was diluted with EtOAc, adsorbed on silica gel (1 g), and the solvent evaporated. Purification by flash chromatography (EtOAc/EtOH 9:1) afforded 78 mg (90%) of **5** as a white foam. R_f 0.38 (EtOAc/EtOH 9:1). ^{1}H NMR (300 MHz, CD_3OD): δ 0.93 (m, 1H), 1.04 (m, 1H), 1.56 (m, 1H), 1.69 (d, 1H, J = 14.3 Hz), 1.90 (dd, 1H, J_1 = 4.8, J_2 = 14.3 Hz), 2.47 (dd, 1H, J_1 = 3.0, J_2 = 14.0 Hz), 2.73 (dd, 1H, J_1 = 7.0, J_2 = 14.0 Hz), 4.31 (s, 1H), 6.14 (dd, 1H, J_1 = 2.6, J_2 = 7.0 Hz), 7.54 (m, 2H), 7.64 (m, 2H), 7.97 (m, 2H), 8.65 (d, 1H, J = 7.7 Hz). ^{13}C NMR (75 MHz, CD_3OD): δ 18.13, 25.33, 42.95, 49.00, 65.20, 86.54, 91.07, 93.10, 98.09, 129.41, 130.04, 134.86, 146.39, 157.83, 165.02, 169.22. IR (KBr): 3397, 1702, 1645, 1485, 1308, 1255 cm^{-1}. MS (LSIMS): *m*/*z* (rel intensity) 370 (17), 341 (30), 216 (100), 155 (40), 119 (65). HRMS (LSIMS): *m*/*z* calcd for $C_{19}H_{20}N_3O_5$, 370.1402; found, 370.1395.

(5′*R*)-(*N*^{4}-Benzoyl-1-[5′-*O*-(4,4′-dimethoxytriphenyl)methyl-2′-deoxy-3′-*C*, 5′-*C*-[(5′-*C*, 6′-*C*-methano)ethano]-β-D-ribofuranosyl]-cytosine (6). To a solution of **5** (175 mg, 0.47 mmol) in pyridine (1.9 mL) was added under stirring DMTOTf (435 mg, 0.95 mmol). After 4, 7, and 10 h, further portions of 1 equiv of DMTOTf were added. The reaction mixture was diluted with EtOAc and extracted with saturated $NaHCO_3$. The organic layers were dried over $MgSO_4$ and concentrated. Purification by flash chromatography (EtOAc/EtOH 9:1 + 1% Et_3N) afforded 277 mg (87%) of **6** as yellow foam. R_f 0.45 (EtOAc/EtOH 9:1). ^{1}H NMR (300 MHz, $CDCl_3$): δ 0.53 (m, 1H), 1.37 (m, 1H), 1.62 (d, 1H, J = 13.6 Hz), 1.76 (m, 2H), 2.24 (s, 1H), 2.52 (d, 2H, J = 4.0 Hz), 2.64 (s, 1H), 3.79, 3.80 (2s, 6H), 5.96 (t, 1H, J = 4.0 Hz), 6.83 (m, 4H), 7.25 (m, 3H), 7.40 (d, 4H), 7.51 (m, 4H), 7.61 (m, 1H), 7.93 (d, 2H), 8.79 (br, 1H), 9.00 (d, 1H, J = 7.4 Hz). ^{13}C NMR (75 MHz, $CDCl_3$): δ 14.16, 25.52, 41.49, 48.41, 54.82, 54.85, 68.06, 86.49, 88.50, 90.21, 92.09, 113.32, 127.15, 128.83, 128.97, 131.40, 132.68, 133.81, 137.45, 137.53, 144.91, 147.29, 159.34, 163.26. IR (film): ν 3028, 1482 cm^{-1}. MS (LSIMS): *m*/*z* (rel intensity) 672 (40), 530 (17), 455 (12). MS (ESI-TOF): *m*/*z* calcd for $[M - H]^-$ = 670.2553; found, 670.2557.

(5′*R*)-(*N*^{4}-Benzoyl-1-[3′-*O*-(2-cyanoethoxy)(diisopropylamino)-phosphino-5′-*O*-(4,4′-dimethoxytriphenyl)methyl-2′-deoxy-3′-*C*, 5′-*C*-[(5′-*C*, 6′-*C*-methano)ethano]-β-D-ribofuranosyl]cytosine (7). 2-Cyanoethyl *N*,*N*-diisopropylchlorophosphoramidite (234 μL, 1.13 mmol) was added dropwise at room temperature to a solution of **6** (253 mg, 0.37 mmol) and *N*,*N*-diisopropylethylamine (0.32 mL, 1.88 mmol) in CH_3CN (2.3 mL). After 2 h, EtOAc was added, and the mixture was

extracted with saturated $NaHCO_3$. The combined organic layers were dried over $MgSO_4$ and concentrated. Flash chromatography (EtOAc + 1% Et_3N) yielded 300 mg (91%) of **7** as a slightly yellow foam (1:1 mixture of diastereoisomers). R_f 0.36, 0.47 (EtOAc). ^{1}H NMR (400 MHz, C_6D_6): δ 0.70 (m, 0.6H), 0.75 (m, 0.4H), 0.95 (m, 1H), 1.10 (m, 12H), 1.33 (m, 2H), 1.57 (m, 1H), 1.83 (m, 2H), 2.06 (d, 1H, J = 14.3 Hz), 2.21 (dd, 1H, J_1 = 3.7, J_2 = 14.3 Hz), 2.68 (dd, 1H, J_1 = 14.0, J_2 = 20.6 Hz), 2.89 (dd, 0.6H, J_1 = 7.0, J_2 = 14.3 Hz), 3.01 (m, 0.4H), 3.04 (s, 0.6H), 3.06 (s, 0.4H), 3.21 (m, 2H), 3.44, 3.45 (2s, 6H), 6.15 (d, 1H, J = 5.1 Hz), 6.90 (m, 4H), 7.13 (m, 4H), 7.31 (m, 3H), 7.65 (m, 5H), 7.80 (d, 2H, J = 7.4 Hz), 7.97 (br, 1H), 9.10 (m, 1H). ^{13}C NMR (100 MHz, C_6D_6): δ 18.05, 20.05, 20.13, 24.40, 24.48, 24.56, 24.64, 24.71, 25.62, 39.65, 43.48, 43.54, 43.61, 43.67, 46.54, 54.99, 58.06, 58.26, 58.39, 58.59, 67.75, 88.87, 88.90, 90.37, 90.44, 90.49, 90.56, 92.38, 92.68, 113.54, 117.67, 117.85, 127.42, 127.42, 128.22, 128.49, 128.89, 131.64, 132.64, 137.56, 137.59, 144.50, 147.35, 147.38, 159.06, 163.42. ^{31}P NMR (161.9 MHz, C_6D_6): δ 143.96, 145.18. IR (KBr): 1663, 1507, 1485, 1244 cm^{-1}. MS (ESI-TOF): *m*/*z* calcd for $[M - H]^-$ = 870.3632; found, 870.3627.

(5′*R*)-(*O*^{6}-Diphenylcarbamoyl-*N*^{2}-isobutyryl-[3′-*O*-trimethylsilyl-5′-*O*-(*tert*-butyldimethylsilyl)-2′-deoxy-3′-*C*, 5′-*C*-[(5′-*C*, 6′-*C*-methano)ethano]-D-ribofuranosyl]guanine (8−10). A suspension of *O*^{6}-diphenylcarbamoyl-*N*^{2}-isobutyrylguanine (1.82 g, 4.35 mmol) in CH_3CN (20 mL) and BSA (4.4 mL, 18.14 mmol) was stirred for 30 min at 40 °C. To the clear solution was added at room temperature **1** (1.09 g, 3.62 mmol) in CH_3CN (10 mL) followed by $CF_3SO_3SiMe_3$ (1.94 mL, 10.86 mmol). The reaction mixture was stirred for 3 h at 50 °C. The reaction was stopped by the addition of EtOAc and extraction with saturated $NaHCO_3$. The combined organic layers were dried over $MgSO_4$ and concentrated. Flash chromatography (hexane/EtOAc 2:1 → EtOAc → MeOH) afforded 528 mg (20%) of **8**, 123 mg (5%) of des-trimethylsilyl-**8**, 195 mg (7%) of **9**, 370 mg (15%) of des-trimethylsilyl-**9**, and 130 mg (5%) **10** (mixture of α- and β-anomers) as white foams. Data of **8**: R_f 0.49 (hexane/EtOAc 2:1). ^{1}H NMR (300 MHz, DMSO-d_6): δ 0.04 (s, 6H), 0.14 (s, 9H), 0.73 (m, 1H), 0.82 (s, 9H), 0.99 (m, 1H), 1.10, 1.12 (2s, 6H), 1.43 (m, 1H), 1.63 (d, 1H, J = 14.0 Hz), 2.04 (m, 1H), 2.66 (dd, 1H, J_1 = 7.4, J_2 = 13.6 Hz), 2.88 (m, 1H), 3.22 (dd, 1H, J_1 = 4.0, J_2 = 13.6 Hz), 4.17 (s, 1H), 6.44 (dd, 1H, J_1 = 3.7, J_2 = 6.2 Hz), 7.33 (m, 2H), 7.45 (m, 8H), 8.62 (s, 1H), 10.71 (s, 1H). ^{13}C NMR (75 MHz, DMSO-d_6): δ −3.91, −3.72, 2.04, 14.23, 17.63, 19.40, 25.68, 45.35, 45.35, 64.76, 86.35, 88.61, 91.96, 121.13, 127.11, 127.40, 129.26, 129.52, 141.75, 143.29, 150.27, 152.27, 154.16, 155.12, 175.15. IR (KBr): 3254, 2970, 1750, 1612, 1245 cm^{-1}. MS (LSIMS): *m*/*z* (rel intensity) 757 (7), 417 (45), 341 (65), 297 (40), 251 (20), 225 (80), 196 (100), 168 (40). Data of **9**: R_f 0.30 (hexane/EtOAc 2:1). ^{1}H NMR (300 MHz, DMSO-d_6): δ 0.04, 0.06 (2s, 6H), 0.11 (s, 9H), 0.77 (s, 9H), 0.80 (m, 1H), 0.97 (m, 1H), 1.10, 1.12 (2s, 6H), 1.56 (m, 1H), 1.78 (d, 1H, J = 13.6 Hz), 2.31 (dd, 1H, J_1 = 4.0, J_2 = 14.0 Hz), 2.74 (m, 1H), 2.91 (m, 2H), 4.51 (s, 1H), 6.34 (t, 1H, J = 7.0 Hz), 7.35 (m, 2H), 7.47 (m, 8H), 8.63 (s, 1H), 10.64 (s, 1H). ^{13}C NMR (75 MHz, DMSO-d_6): δ −3.88, −3.64, 1.99, 16.90, 17.68, 19.35, 19.44, 23.79, 25.75, 34.52, 39.63, 44.72, 65.38, 87.03, 84.14, 89.52, 120.85, 127.11, 127.41, 129.29, 129.57, 141.76, 143.60, 144.24, 150.36, 152.43, 154.42, 155.24, 175.03. IR (KBr): 2920, 1721, 1250 cm^{-1}. MS (LSIMS): *m*/*z* (rel intensity) 757 (25), 417 (60), 341 (55), 225 (50), 196 (100), 168 (35).

(5′*R*)-(*N*^{2}-Isobutyryl-9-[5′-*O*-(*tert*-butyldimethylsilyl)-2′-deoxy-3′-*C*, 5′-*C*-[(5′-*C*, 6′-*C*-methano)ethano]-β-D-ribofuranosyl]guanine (11). A solution of **9** (518 mg, 0.68 mmol) in DMSO (5 mL) was treated with saturated $NaNO_2$ in DMSO (15 mL) and stirred for 10 h at 60 °C. The reaction mixture was diluted with EtOAc at room temperature, and the precipitate was filtered off. The recovered solution was concentrated, and the residue was purified by flash chromatography (CH_2Cl_2/MeOH 20:1 → 10:1) to afford 302 mg (90%) of **11** as a yellow oil. R_f 0.26 (CH_2Cl_2/MeOH 20:1). ^{1}H NMR (300 MHz, CD_3OD): δ 0.18, 0.24 (2s, 6H), 0.83 (m, 1H), 0.95 (s, 9H), 1.12 (m, 1H), 1.24, 1.27 (2s, 6H), 1.45 (m, 1H), 1.62 (d, 1H, J = 14.0 Hz), 1.72 (dd, 1H, J_1 = 4.8, J_2 = 14.3 Hz), 2.74 (m, 2H), 2.92 (dd, 1H, J_1 = 2.2, J_2 = 13.6 Hz), 4.31 (s, 1H), 6.35 (dd, 1H, J_1 = 2.2, J_2 = 6.6 Hz), 8.50 (s, 1H). ^{1}H NMR difference NOE: 1.45 (m, 1H) → 8.50 (s, 1H); 4.31 (s, 1H) → 0.83 (m, 1H), 2.74 (m, 2H), 6.35 (dd, 1H, J_1 = 2.2, J_2 = 6.6 Hz); 6.35 (dd, 1H, J_1 = 2.2, J_2 = 6.6 Hz) → 2.74 (m, 2H), 4.31 (s, 1H), 8.50 (s, 1H); 8.50 (s, 1H) → 1.45 (m, 1H), 6.35 (dd, 1H, J_1 = 2.2, J_2 = 6.6 Hz). ^{13}C NMR (75 MHz, CD_3OD): δ −3.19, −3.13, 18.66, 19.03, 19.66, 19.67, 26.30, 37.27, 42.75, 49.10, 67.10, 88.01, 89.10, 93.61, 122.44, 139.60, 139.70, 149.79, 157.81, 182.04. MS (ESI-TOF): *m*/*z* calcd for $C_{23}H_{34}N_5O_5Si$, 488.2329; found, 488.2326.

(5′*R*)-(*N*^{2}-Isobutyryl-9-[2′-deoxy-3′-*C*, 5′-*C*-[(5′-*C*, 6′-*C*-methano)-ethano]-β-D-ribo-furanosyl]guanine (12). A solution of **11** (145 mg, 0.30 mmol) in THF (6 mL) and HF Et_3N (0.3 mL, 0.59 mmol) was stirred for 8 h. Silica gel (0.5 g) was added, and the solvent evaporated to dryness. Flash chromatography (EtOAc/EtOH 4:1 → 3:2) yielded 68 mg (61%) of **12** as a yellow solid. R_f 0.51 (CH_2Cl_2/MeOH 5:1). ^{1}H NMR (300 MHz, CD_3OD): δ 0.86 (m, 1H), 1.04 (m, 1H), 1.24, 1.27 (2s, 6H), 1.54 (m, 1H), 1.66 (d, 1H, J = 14.0 Hz), 1.95 (dd, 1H, J_1 = 5.1, J_2 = 14.0 Hz), 2.70 (m, 2H), 2.79 (dd, 1H, J_1 = 4.0, J_2 = 13.6 Hz), 4.24 (s, 1H), 6.36 (dd, 1H, J_1 = 4.0, J_2 = 6.6 Hz), 8.42 (br, 1H). ^{13}C NMR (75 MHz, DMSO-d_6): δ 17.29, 19.04, 19.39, 23.26, 34.86, 41.29, 47.12, 63.11, 85.33, 85.38, 90.80, 121.00, 137.43, 147.91, 147.99, 154.99, 180.24. IR (KBr): 3240, 2965, 1676, 1611 cm^{-1}. MS (LSIMS): *m*/*z* (rel intensity) 376 (4), 242 (100), 222 (12). HRMS (LSIMS): *m*/*z* calcd for $C_{17}H_{22}N_5O_5$, 376.1620; found, 376.1613.

(5′*R*)-(*N*^{2}-Isobutytryl-9-[5′-*O*-(4,4′-dimethoxytriphenyl)methyl-2′-deoxy-3′-*C*, 5′-*C*-[(5′-*C*, 6′-*C*-methano)ethano]-β-D-ribofuranosyl]-guanine (13). To a solution of **12** (76 mg, 202 μmol) in pyridine (0.7 mL) was added at room temperature (in four portions over 8 h) DMTOTf (348 mg, 707 μmol). After another 2 h, the reaction mixture was diluted with CH_2Cl_2 and the mixture extracted with saturated $NaHCO_3$. The combined organic layers were dried over $MgSO_4$ and concentrated. Flash chromatography (CH_2Cl_2/MeOH 15:1 → 10:1 + 0.02% Et_3N) afforded 114 mg (83%) of **13** as a brown solid. R_f 0.62 (CH_2Cl_2/MeOH 10:1). ^{1}H NMR (300 MHz, CD_3OD): δ 0.50 (m, 1H), 0.92 (m, 1H), 1.24 (2s, 6H), 1.59 (m, 1H), 1.75 (m, 1H), 2.44 (dd, 1H, J_1 = 6.6, J_2 = 13.6 Hz), 2.67 (s, 1H), 2.74 (m, 1H), 3.24 (m, 1H), 3.80, 3.81 (2s, 6H), 6.17 (d, 1H, J = 5.1 Hz), 6.87 (m, 4H), 7.26 (m, 3H), 7.43 (m, 4H), 7.53 (m, 2H), 8.81 (s, 1H). ^{13}C NMR (75 MHz, $CDCl_3$): δ 17.17, 19.06, 19.43, 23.27, 34.90, 40.65, 47.21, 55.24, 67.46, 85.98, 87.33, 86.87, 90.97, 113.00, 113.06, 121.53, 127.02, 127.76, 128.35, 130.63, 130.74, 136.88, 136.98, 146.58, 147.54, 148.06, 155.09, 158.46, 158.53, 180.41. IR (KBr): 3400, 3130, 1678, 1607, 1250 cm^{-1}. MS (LSIMS): *m*/*z* (rel intensity) 678 (9), 335 (12), 303 (100).

(5′*R*)-(*N*^{2}-Isobutyryl-9-[3′-*O*-(2-cyanoethoxy)(diisopropylamino)-phosphino-5′-*O*-(4,4′-dimethoxytriphenyl)methyl-2′-deoxy-3′-*C*, 5′-*C*-[(5′-*C*, 6′-*C*-methano)ethano]-β-D-ribofuranosyl]guanine (14). 2-Cyanoethyl *N*,*N*-diisopropylchlorophosphoramidite (77 μL, 0.33 mmol) was added dropwise at room temperature to a solution of **13** (114 mg, 0.17 mmol) and *N*,*N*-diisopropylethylamine (114 μL, 0.17 mmol) in CH_3CN (0.4 mL) and THF (1.1 mL). After 5 h and 6 h, further portions of 1 equiv of 2-cyanoethyl *N*,*N*-diisopropylchlorophosphoramidite were added. After 10 h, 2-propanol was added, and the reaction mixture was extracted with saturated $NaHCO_3$. The combined organic layers were dried over $MgSO_4$ and concentrated. Flash chromatography (CH_2Cl_2/acetone 3:1 + 0.02% Et_3N) yielded 129 mg of **14** as a yellow oil. Repeated precipitation from CH_2Cl_2 (0.3 mL) in hexane (100 mL) at 0 °C afforded 85 mg (58%) of **14** as a slightly brownish powder (3:2 mixture of diastereoisomers). R_f 0.60 (CH_2Cl_2/acetone 3:1). ^{1}H NMR (400 MHz, $CDCl_3$): δ 0.43 (m, 1H), 1.06 (m, 12H), 1.15 (m, 1H), 1.24 (m, 6H), 1.35 (m, 1H), 1.52 (m, 0.4H), 1.71 (m, 1H), 2.15 (dd, 0.6H, J_1 = 6.0, J_2 = 14.7 Hz), 2.60 (m, 4H), 3.18 (t, 1H, J = 13.9 Hz), 3.42 (m, 4H), 3.79 (s, 6H), 6.03 (dd, 1H, J_1 = 5.2, J_2 = 12.1 Hz), 6.80 (m, 5H), 7.22 (m, 1H), 7.44 (m, 5H), 7.51 (m, 2H), 8.62 (s, 1H), 8.72 (s, 0.4H), 8.99 (s, 0.6H), 11.91 (s, 1H). ^{13}C NMR (100 MHz,

$CDCl_3$): δ 16.73, 16.94, 18.62, 18.72, 20.36, 20.44, 24.29, 24.95, 36.18, 38.28, 38.43, 42.71, 42.83, 42.94, 45.58, 55.08, 56.78, 56.85, 56.96, 57.03, 67.28, 67.40, 87.60, 88.36, 91.21, 92.17, 87.79, 87.85, 89.77, 89.83, 90.12, 112.74, 117.70, 122.34, 126.73, 127.54, 128.46, 130.55, 130.81, 137.01, 137.27, 137.78, 146.27, 146.54, 146.85, 155.56, 155.63, 158.45, 158.52, 178.26, 178.45. ^{31}P NMR (161.9 MHz, $CDCl_3$): δ 142.71, 142.88. IR (KBr): 3404, 2971, 1670, 1613, 1255 cm^{-1}.

X-ray Structures of 3 and 15. Data of **3**. Crystal shape, rod; crystal color, colorless; crystal size, 0.5 × 0.3 × 0.2 mm^3; empirical formula, $C_{25}H_{33}N_3O_5Si$ (MW = 483.63); crystal system, orthorhombic; space group, $P2_12_12_1$; unit cell dimensions (Å), a = 6.2225(4), b = 11.3686(6), c = 35.120(2), α = 90°, β = 90°, γ = 90°; volume, 2484.4(3) $Å^3$; reflections, 8000 (plus equivalents); angle range, 1.88 < θ < 25.92; Z, 4; density (calc.), 1.293 g/cm^3; radiation used, Mo Kα; wavelength, 0.71073 Å; linear absorption coefficient, 0.135 mm^{-1}; temperature, 153(2) K; number of reflections measured, 16 272; number of independent reflections, 4738; number of observed reflections, 3898; R(int.) = 0.0654; F(000), 1032. Data of **15**. Crystal shape, rod; crystal color, colorless; crystal size, 0.5 × 0.3 × 0.2 mm^3; empirical formula, $C_{24}H_{31}N_5O_6$ (MW = 485.54); crystal system, orthorhombic; space group, $P2_12_12_1$; unit cell dimensions (Å), a = 7.6651(5), b = 13.3047(7), c = 23.7387(12), α = 90°, β = 90°, γ = 90°; volume, 2420.9(2) $Å^3$; reflections, 6776 (plus equivalents); angle range, 2.30 < θ < 25.92; Z, 4; density (calc.), 1.332 g/cm^3; radiation used, Mo Kα; wavelength, 0.71073 Å; linear absorption coefficient, 0.097 mm^{-1}; temperature, 153(2) K; number of reflections measured, 9936; number of independent reflections, 4663; number of observed reflections, 3069; R(int.) = 0.0382; F(000), 1032.

Oligonucleotide Synthesis and UV Melting Experiments. Syntheses of oligonucleotides were performed with solid-phase phosphoramidite methodology on the 1.0 or 1.3 μmol scale using a Pharmacia LKB Gene Assembler Special instrument. CH_3CN was distilled over CaH_2 and stored under activated molecular sieves (3 Å). The assembly of tricyclo-DNA was performed according to the standard synthesis cycles (trityl off mode) with the exception of a prolonged coupling time (10 min) and an 11-fold instead of a 9-fold molar excess of phosphoramidites. Because of solubility reasons, $ClCH_2CH_2Cl$ was used as the solvent for the tricyclodeoxyadenosine building block and a mixture of CH_3CN/THF = 3:1 for the tricyclodeoxyguanosine building block. In the coupling step, tetrazole (0.45 M in CH_3CN) was replaced by the more active 5-(benzylmercapto)-1*H*-tetrazole (0.25 M in CH_3CN) or 5-(ethylmercapto)-1*H*-tetrazole (0.25 M in CH_3CN). For sequences **20**−**23**, the universal solid support from CT-Gen (San Jose) was used, and for all other oligonucleotides the standard CPG-solid supports from Glen Research were used. The 5′-ends of oligotricyclodeoxynucleotides were equipped with a phosphate group by terminal coupling with the phosphorylating reagent 2-[2-(4,4′-dimethoxytrityloxy)ethylsulfonyl]ethyl-(2-cyanoethyl)-(*N*,*N*-diisopropyl)-phosphoramidite (Glen Research). For comparison, the natural oligonucleotides were synthesized in the same way. After synthesis, the solid support was suspended in concentrated NH_3 solution (ca. 1 mL) and left overnight at 55 °C, or for 63 h at 60−65 °C in those cases where the universal solid support was used. The crude oligonucleotides were purified by anion-exchange HPLC (Macherey-Nagel, Nucleogen DEAE 60/7) and desalted over SEP-PAK C-18 cartridges (Waters). Their purity was controlled by RP-HPLC and estimated to be ≥95%. All oligodeoxynucleotides were routinely analyzed by ESI mass spectrometry. The corresponding MS data are given in Figure 3.

UV Melting Curves. UV melting curves were determined at 260 nm on a Varian Cary 3E spectrophotometer that was equipped with a Peltier block using the Varian WinUV software. Complementary oligodeoxynucleotides were mixed to 1:1 stoichiometry with a 2 μM single strand oligonucleotide concentration. A heating−cooling−heating cycle (0 → 90 °C) was applied with a temperature gradient of 0.5 °C/min. T_m values were defined as the maximum of the first derivative of the melting curve using the software package Origin 5.0. Thermodynamic data for duplex formation were obtained as indicated in the text.

CD Spectra. CD spectra were recorded on a Jasco J-715 spectropolarimeter with a Jasco PFO-350S temperature controller. The temperature was measured directly in the cell (path length 10 mm).

Molecular Modeling. Molecular modeling calculations were carried out with the Amber force field as incorporated in the software package Insight II/Discover 3 V98.0 of Molecular Simulations, Inc. on an SGI Octane workstation. Only original Amber parameters and potentials were used. No explicit H_2O molecules and counterions were included. A distance-dependent permittivity of $\epsilon = 4r$ was used instead as a screening function. One to four nonbonded interactions were scaled by 0.5. No cutoffs were applied. Structures were built on the basis of the parameters of a B-DNA double helix. They were first minimized until the energy gradient was below 0.05 kcal/mol Å. The structures were then heated stepwise from 0 to 300 K over 20 ps (1 ps at 50 K, 1 ps at 100 K, 2 ps at 150 K, 2 ps at 200 K, 4 ps at 250 K, and 10 ps at 300 K) and submitted to 200 ps of unrestrained molecular dynamics at 300 K. The temperature was controlled by coupling to an external heat bath. One-fs time steps were used in the numerical integration of the equation of motion. For the analysis, coordinates and energy terms were stored every 0.5 ps.

Acknowledgment. We thank the BENEFRI Small Molecule Crystallography Service directed by Prof. Helen Stoeckli-Evans for measuring the X-ray data sets. Financial support of this work by the Swiss National Science Foundation (grant 20-63582.00) is gratefully acknowledged.

Supporting Information Available: Experimental details on the synthesis of the tricyclo-G nucleosides with *O*-6-phenethyl-*N*-2-isobutyrylguanine as the base synthon (PDF). This material is available free of charge via the Internet at http://pubs.acs.org.

JA025569+